ONLINE SUPPLEMENT TO

THE ROLE OF CARBONIC ANHYDRASE 9 IN REGULATING EXTRACELLULAR AND INTRACELLULAR pH IN 3-D TUMOR-CELL GROWTHS

Supplemental figure legends

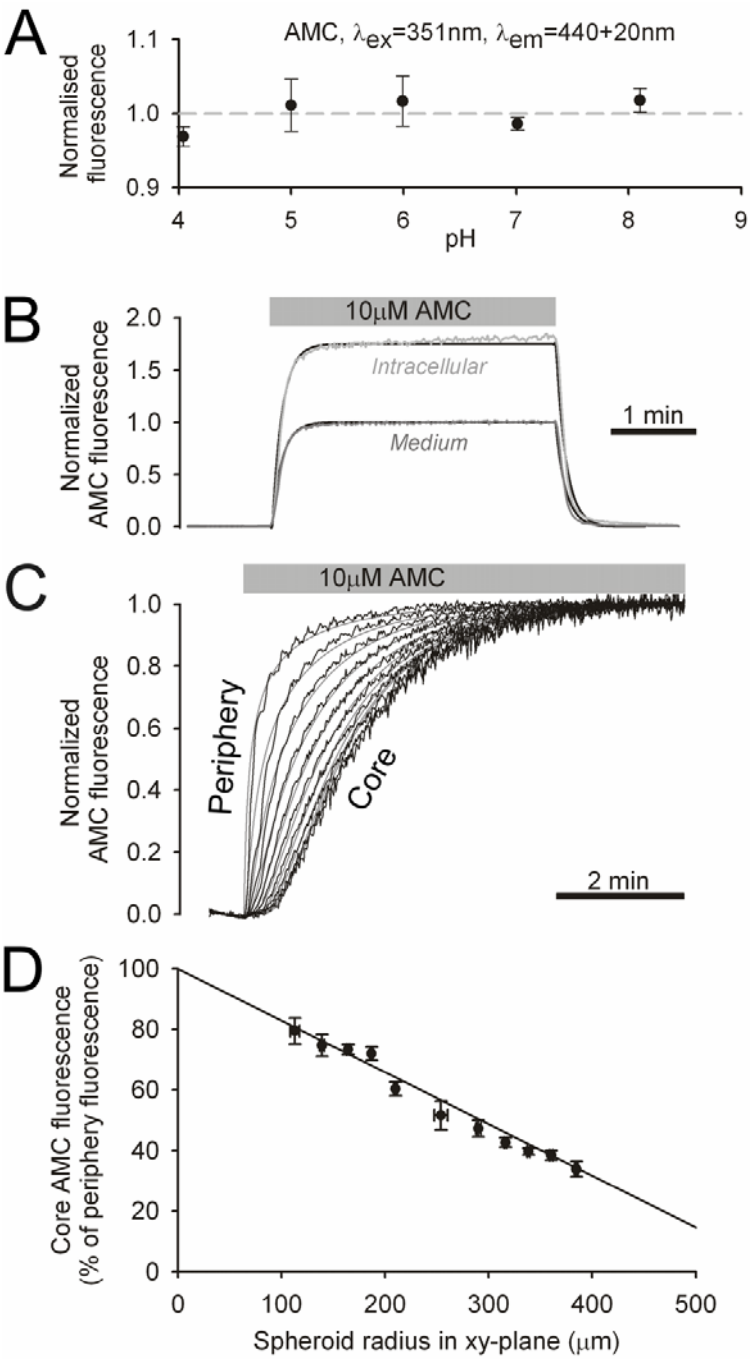

Supplemental Figure S1: *Characterizing spheroid geometry with the fluorescent dye, 7-amino-4-methylcoumarin (AMC).* AMC was excited at 351nm and fluorescence was collected confocally at 440±20nm. (A) Fluorescence from 10μM AMC solution (cell-free) showed no pH-sensitivity. (B) Single cells superfused with 10μM AMC solution. Intracellular AMC fluorescence increases rapidly, indicating high membrane-permeability of the dye (10μm/s). At steady-state, intracellular AMC fluorescence was 1.8-fold higher than medium fluorescence, possibly as a consequence of interactions between dye and proteins or nucleic acids. (C) Spheroids (radius 305±33μm) superfused with 10μM AMC solution. Total (intra- and extracellular) AMC fluorescence time-courses in ten ROIs show that the rise in signal at the spheroid core lagged behind the rise at its periphery, in agreement with an effective AMC diffusion coefficient of 212±12μm^2/s. This is 4.8-fold lower than AMC mobility in aqueous solution at 37°C. Using a bi-domain diffusion model (featuring flux between intra- and extracellular spheroid compartments but diffusion only across the extracellular space), this mobility predicts that 80% of spheroid volume is intracellular and the rest is restricted extracellular space. This is close to the 74% predicted from Kepler's conjecture for close packing of spheres into larger spheres. (D) In the xy-plane, the ratio of minor-to-major radius was 0.92±0.03, suggesting good radial symmetry. Core AMC fluorescence (normalized to periphery fluorescence) decreased linearly with xy-plane spheroid radius, due to signal attenuation by the tissue-mass. The linear relationship suggests that the radius in the z-axis direction is proportional to that in the xy-plane. These data show that spheroids show a high degree of spherical symmetry.

Supplemental Figure S2: *Imaging spheroids with fluorescein-derivatives*. (A) CA9-expressing spheroid (radius 250µm) exposed to 30µM fluorescein-5-(and-6-)-sulfonic acid (FS) solution for 4min. Fluorescence excited at 488nm and detected >515nm. Due to membrane-impermeability, FS signal is extracellular-only. Fluorescence time-courses were averaged in ten concentric ROIs and normalized to steady-state fluorescence. For clarity, only the time-courses in odd-numbered ROIs are shown. The initial, rapid addition or removal of superfusate FS is not detected at the core of spheroids (ROI1), therefore the system does not pick-up significant bleed-through of fluorescence from above and below the confocal plane. (B) CA9-expressing spheroid, imaged with FS excited at (i) 458nm and (ii) 488nm. (iii) ratio of (i) and (ii), revealing low pH_e at the spheroid core. (C) Radial profiles of FS ratio in CA9-expressing spheroids (*black squares;* n=20; radius 250-350µm) and EV spheroids (*red circles;* n=20; radius 250-350µm). Radially-decreasing FS ratio is indicative of a pH_e gradient of pH_e. Core pH_e was more acidic in CA9-expressing spheroids. Also shown is the fluorescence ratio of 5-(and-6-)-carboxy-2',7'-dichlorofluorescein (CCF), a dye with acid-shifted pK (=4.8). The dye is effectively pH-insensitive over the range pH_e 6-8.

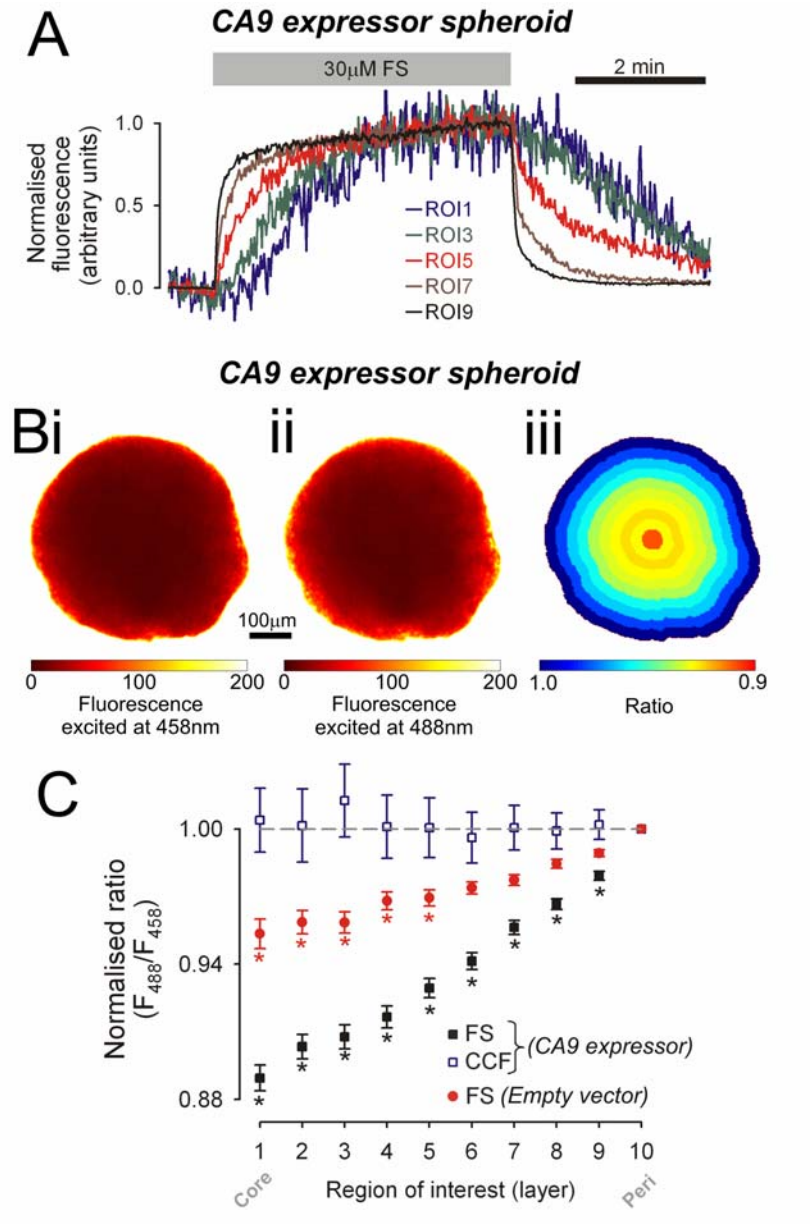

Supplemental Figure S3: *Cellular metabolic acid-output measured from medium acidification.* Cells transfected with CA9 or empty vector (EV) were grown in 4.2mL DMEM culture medium with 11mM glucose, buffered by 20mM Hepes. Incubation was performed in nominally CO_2/HCO_3^--free conditions to mimic a closed buffer system and thereby minimize the loss of acid in the form of volatile CO_2. Flasks were incubated at 37°C and under a 20% O_2 (nominally CO_2-free) atmosphere. Twenty flasks were run in parallel (ten with EV and ten with CA9-expressing cells). After 20, 44, 68, 142 or 167hrs of incubation, medium pH was measured and cells were liberated with trypsin for counting under a hemocytometer. Figure shows medium pH against cell count. No significant difference was detected between CA9-expressor cells versus EV cells. Therefore, expression of the CA9 gene does not alter overall metabolic acid-output.

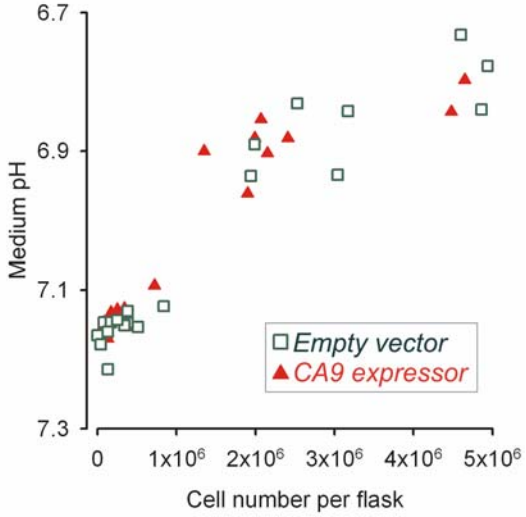

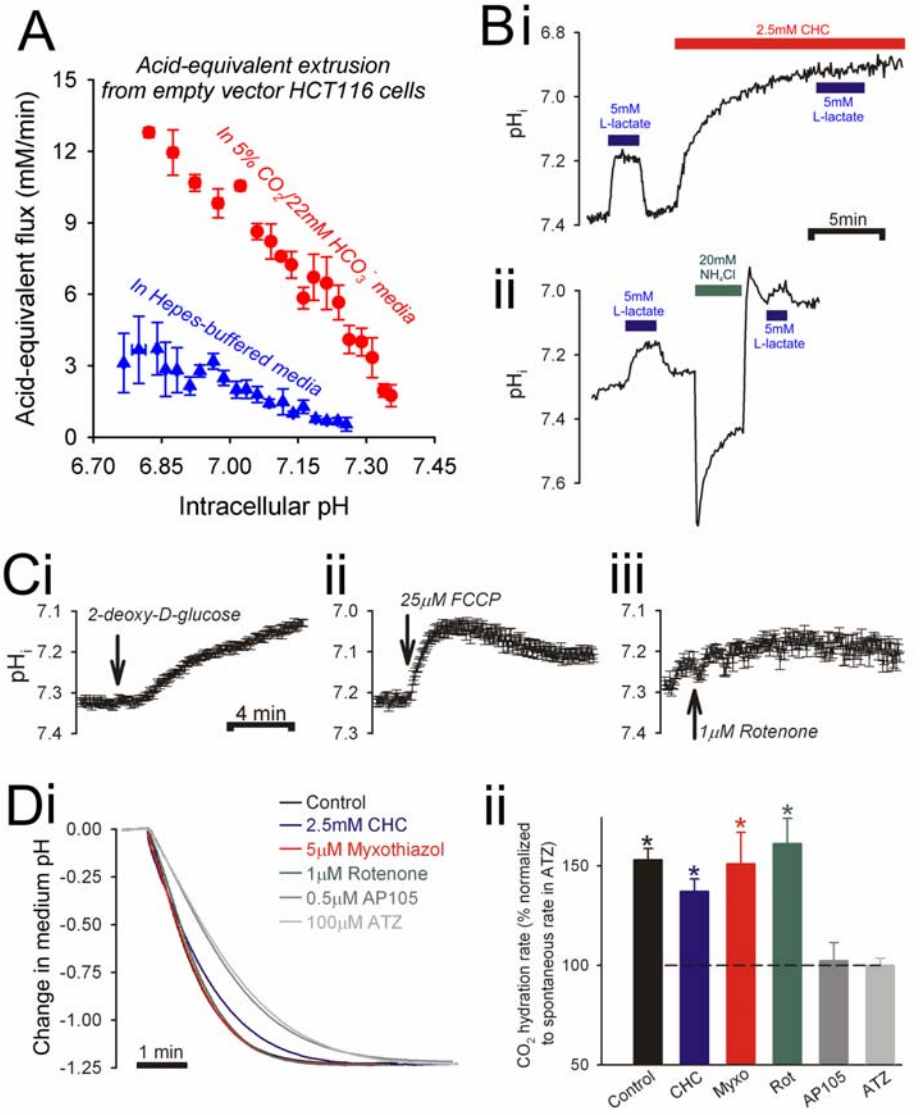

Supplemental Figure S4: (A-B) *Regulation of pH_i by acid-equivalent membrane transport in HCT116 cells.* Cells were loaded with carboxy-SNARF-1 to measure pH_i. (A) Acid-equivalent transmembrane flux was measured in the presence (*red*) and absence (*blue*) of extracellular CO_2/HCO_3^- buffer. To stimulate acid-extrusion, pH_i was reduced by means of a 20mM ammonium prepulse. The rate of pH_i recovery was converted to acid-equivalent flux and plotted as a function of pH_i. This flux was low in the absence of extracellular HCO_3^-, indicating that H^+-ion extrusion on transporters such as Na^+/H^+ exchange is slow. In the presence of extracellular HCO_3^-, flux is greatly enhanced, indicating a high level of HCO_3^- uptake on HCO_3^- transporters. (B). The presence of monocarboxylic acid transport (MCT) was assessed by measuring pH_i changes in single cells exposed transiently to solution containing 5mM sodium lactate. All solutions were buffered with 20mM Hepes-buffered media at pH 7.4 (37°C). (i) After a control lactate pulse, cells were superfused with the MCT inhibitor, α-cyanohydroxy-cinnamate (CHC), which acidified pH_i *per se*. Subsequent transient exposure to 5mM sodium lactate (+CHC) did not change pH_i in CHC-pretreated cells. (ii) In a different cell, a control lactate pulse was followed by an ammonium prepulse that acidified pH_i to the levels attained with CHC alone. A subsequent lactate pulse at the reduced pH_i still produces a measureable pH_i change. These data indicate that a considerable fraction of lactic acid flux across the cell membrane occurs via MCT. The time-course of pH_i acidification was used to best-fit an 'effective', MCT-facilitated membrane permeability to lactic acid of P_{HLac}=250μm/s. (C-D) *Measuring the effect of inhibitors used in the present study on resting pH_i and carbonic anhydrase activity.* (C) Single cells were superfused with 5% CO_2/22mM HCO_3^- buffered media. At 2min, superfusate was switched rapidly to (i) one containing 11mM 2-deoxy-D-glucose, (ii) containing 25μM FCCP, or (iii) containing 1μM rotenone. (D) (i) The kinetics of CO_2 hydration were estimated from the time-course of medium acidification on addition of CO_2-saturated water, as outlined in Fig. 1D. In the presence of CA9 from the membranes of CA9-expressing cells, CO_2 hydration was accelerated. (ii) Catalysis by CA9 was blocked by ATZ and AP105, but not by CHC, myxothiazol (myxo) or rotenone (rot).

3-D diffusion-reaction model for extracellular pH regulation in spheroids

Geometry. The diffusion-reaction equations were solved over a sphere Ω of radius R, consisting of an intracellular space Ω_i occupying volume fraction V_i and extracellular space Ω_e occupying volume fraction $V_e=1-V_i$ (1). The intracellular space Ω_i represents the union of all cells (radius r) and the extracellular space Ω_e is continuous throughout the spheroid. $\Omega=\Omega_i\cup\Omega_e$. Therefore, diffusion is allowed in Ω_e but not in Ω_i. This continuum approximation is permitted as r<<R. The surface area/volume ratio of single cells is ρ.

Exchange between domains. Flux from Ω_e to Ω_i is given by the general formula $J_X=\rho\times P_X\times([X]_i-[X]_e)$, where P is a permeability constant and [X] denotes concentration. Flux in the opposite direction is $-J_X\times V_e/V_i$ (1).

Sources of acid. The spheroid's mathematical representation is simplified to that of a cluster of cells that respire substrate at a rate F_{subs}. F_{subs} is assumed to be uniform across the spheroid, approximating the near-uniform [glucose] measured in spheroids (2). Glucose is metabolized aerobically or anaerobically, producing six CO_2 or two lactic acid molecules, respectively. The fraction of aerobic respiration of glucose is given by an exponential decay function, describing the fractional fall of oxygen across the spheroid radius (x), $\exp(-x/\lambda_{O2})$. The rate of CO_2 production from mitochondria (aerobic respiration) is $J_{mito}=F_{subs}\times6\times\exp(-x/\lambda_{O2})$. The rate of lactic acid production from anaerobic respiration is $F_{subs}\times2\times(1-\exp(-x/\lambda_{O2}))$. We have assumed that a fraction of lactic acid is titrated by intracellular HCO_3^- and leaves the cell as CO_2 across the membrane (J_{titr}). Titration of lactic acid by intracellular HCO_3^- requires a continuous supply of HCO_3^- from the extracellular space at a matching rate ($-J_{titr}$). The remainder of lactic acid leaves the cell across the membrane, as H^+-lactate aboard monocarboxylic acid transporter or as H^+-ions extruded by transporters such as Na^+/H^+ exchange (J_{extr}). HCT116 cells express only low levels of NHE activity, therefore the majority of J_{extr} is likely to be MCT-mediated. The kinetics of MCT can be simplified to a permeation process, with permeability constant P_{HLac}. These fluxes are summarized in Figure 6A. The diffusion coefficients of HLac, Lac, CO_2 and HCO_3^- in Ω_e are D_{HLac}, D_{Lac}, D_{CO2} and D_{HCO3}.

Non-CO_2/HCO_3^- buffering. Buffering inside cells is assumed to be pH_i-insensitive and constant at β_i. Extracellular buffering is quantified with pH_e-insensitive capacity β_e plus mobile buffering from Hepes/Mes buffer, where present, at β_{mob}. Hepes/Mes mobility is given by diffusion coefficient D_{mob}. Overall extracellular H^+ mobility (D_H) in the absence of Hepes/Mes is given by D_e, a lump value for effective H^+ mobility and its facilitation by the dye. Effective H^+ mobility in the presence of Hepes/Mes buffer is therefore,

$$D_H=(D_e\times\beta_e+D_{mob}\times\beta_{mob})/(\beta_e+\beta_{mob}).$$

CO_2/HCO_3^- buffering. The components of CO_2/HCO_3^- (carbonic) buffer exist in dynamic equilibrium inside and outside cells: $CO_2+H_2O\Leftrightarrow HCO_3^-+H^+$. The forward and reverse reaction rate constants are k_f and k_r, respectively. The buffer equilibrium constant is K_{CO2}. Without catalysis, the reaction kinetics are slow and therefore the buffer can be driven out-of-equilibrium, particularly during rapid fluxes of HCO_3^-, CO_2 or H^+. To accelerate the reaction, cells express carbonic anhydrase (CA) isoforms either inside cells or on their extracellular-facing surface. The catalytic constant for the intra- and extracellular space is ca_i and ca_e, respectively.

Equations. The diffusion-reaction problem (1) is a system of ten equations describing a vector $u=[u_1, u_2,\ldots u_{10}]$ of solute concentrations in Ω_i and Ω_e. These equations describe $u_1=[H^+]$, $u_2=[HCO_3^-]$, $u_3=[CO_2]$, $u_4=[Lac]$ and $u_5=[HLac]$ in Ω_i, and $u_6=[H^+]$, $u_7=[HCO_3^-]$, $u_8=[CO_2]$, $u_9=[Lac]$ and $u_{10}=[HLac]$ in Ω_e. Due to spherical symmetry, the mathematics simplify to a 1-dimensional diffusion-reaction problem in the radial axis, x.

$$\frac{d\vec{u}}{dt}=\vec{D}\times\frac{d^2\vec{u}}{dx^2}+\vec{R}$$

Vector D describes the diffusion coefficients, $[D_H, D_{HCO3}, D_{CO2}, D_{Lac}, D_{HLac}, 0, 0, 0, 0, 0]$. Vector R describes the reaction fluxes between solutes. These fluxes are:

$$\frac{ca_e\times\left(k_f\times u_3-k_r\times u_1\times u_2\right)+\left(k_-\times u_5-k_+\times u_1\times u_4\right)}{\beta_e/\left(\ln10\times u_1\right)}$$

$$ca_e\times\left(k_f\times u_3-k_r\times u_1\times u_2\right)-\left(V_e/V_i\right)\times J_{titr}$$

$$ca_e\times\left(k_r\times u_1\times u_2-k_f\times u_3\right)+\left(V_e/V_i\right)\times\rho\times P_{CO2}\times\left(u_8-u_3\right)$$

$$\left(k_-\times u_5-k_+\times u_1\times u_4\right)$$

$$\frac{\left(k_+ \times u_1 \times u_4 - k_- \times u_5\right) + \left(V_e / V_i\right) \times \rho \times P_{HLac} \times \left(u_{10} - u_5\right)}{\beta_i / \left(\ln 10 \times u_6\right)}$$

$$ca_i \times \left(k_f \times u_8 - k_r \times u_6 \times u_7\right) + J_{titr}$$

$$ca_i \times \left(k_r \times u_6 \times u_7 - k_f \times u_8\right) + J_{mito} + \rho \times P_{CO2} \times \left(u_3 - u_8\right)$$

$$\left(k_- \times u_{10} - k_+ \times u_6 \times u_9\right)$$

$$\left(k_+ \times u_6 \times u_9 - k_- \times u_{10}\right) + J_{mct} + \rho \times P_{HLac} \times \left(u_5 - u_{10}\right)$$

Boundary conditions. Experimentally, the spheroid surface is in contact with the superfusate, a well-stirred, equilibriated and constant solution. To model this, the boundary condition at x=R is that of reflection for all solutes within Ω_i and Dirichlet constant-value boundary conditions for solutes in Ω_e. Boundary conditions for extracellular solutes therefore equal their concentration in superfusate.

Parameterizing equations and best-fitting to experimental data. The diffusion-reaction model has 28 variables and constants. These parameters are listed in Table 1. There are three reference sources for the parameters: (*a*) previous literature, (*b*) formula (constrain within the parameter set), and (*c*) present data-set. For some cases, parameters were derived directly from data with one-variable fitting. In other, more complex cases (F_{subs}, λ_{O2}, ca_e, D_{mob}, D_e, β_e), parameters were derived by multi-variable fitting, within the range measured or predicted for spheroids.

Table S1: *Variables and constants in the model.*

Symbol	***Value***	***Reference***
r	8.65μm	Figure 2
ρ	3/r	Formula
R	300μm (*unless varied*)	Figures 3-5
V	$4/3\times\pi\times r^3$	Formula
V_e	0.2	Figure S1
V_i	0.8	Figure S1
P_{HLac}	250μm/s	Figure S4Bi
D_{Lac}	$1300\mu m^2/s$	(3,4)
D_{HLac}	$1300\mu m^2/s$	(3,4)
K_{Lac}	10^{-4} M	(4)
k_-	10^6 s^{-1}	Not limiting
k_+	10^{10} M^{-1} s^{-1}	Formula, $k_-=K_L\times k_+$
P_{CO2}	10μm/s	Figure 2B
K_{CO2}	$10^{-6.12}$ M	(1,5)
k_f	0.14 s^{-1}	Figure 2C, (5)
k_r	1.85×10^5 M^{-1} s^{-1}	Formula, $k_f=K_{CO2}\times k_r$
ca_i	4	Figure 2C
ca_e	10 (*unless varied*)	Figure 6B-E
β_i	25mmol/(L cytosol)	Figure 2B
β_e	10mmol/(L extracellular space) =2mmol/(L spheroid)	Figure 6C, E
D_e	$1600\mu m^2/s$	Present data
β_{mob}	0.7×[Hepes, Mes]	Formula, mean for pH 6-7.5
D_{mob}	$1000\mu m^2/s$	Estimate from Fig 5E
D_{HCO3}	$1600\mu m^2/s$	(1,3,4)
D_{CO2}	$2400\mu m^2/s$	(1,3)
λ_{O2}	250μm	150-650μm (2,6)
F_{subs}	90μM/s	30-190μM/s (2,7)

Additional References

1. Swietach, P., Wigfield, S., Cobden, P., Supuran, C. T., Harris, A. L., and Vaughan-Jones, R. D. (2008) *J Biol Chem* **283**(29), 20473-20483
2. Kunz-Schughart, L. A., Doetsch, J., Mueller-Klieser, W., and Groebe, K. (2000) *Am J Physiol Cell Physiol* **278**(4), C765-780
3. Swietach, P., Zaniboni, M., Stewart, A. K., Rossini, A., Spitzer, K. W., and Vaughan-Jones, R. D. (2003) *Prog Biophys Mol Biol* **83**(2), 69-100
4. Vanysek, P. (1999) Ionic conductivity and diffusion at infinite dilution. In: Linde, D. R. (ed). *Handbook of chemistry and physics*, 79th Ed., CRC Press, London
5. Leem, C. H., and Vaughan-Jones, R. D. (1998) *J Physiol* **509 (Pt 2)**, 471-485
6. Carlsson, J., and Acker, H. (1988) *Int J Cancer* **42**(5), 715-720
7. Walenta, S., Doetsch, J., Mueller-Klieser, W., and Kunz-Schughart, L. A. (2000) *J Histochem Cytochem* **48**(4), 509-522